Ceramics International xxx (xxxx) xxx

Contents lists available at ScienceDirect

Ceramics International

journal homepage: www.elsevier.com/locate/ceramint

Generation of mesoporous n-p-n (ZnO–CuO–CeO_2) heterojunction for highly efficient photodegradation of micro-organic pollutants

Muhammad Aadil [a,*], Tehmina Kousar [b], Mehtab Hussain [b], H.H. Somaily [c,i], Aliaa Kareem Abdulla [d], Eman Ramzy Muhammad [e], Eman A.Al-Abbad [f], Mohamed Abdel Salam [g], Soha M.Albukhari [g], Doaa F. Baamer [g], Mohd Zahid Ansari [h,**]

[a] Department of Chemistry, Rahim Yar Khan Campus, The Islamia University of Bahawalpur, Pakistan
[b] Institute of Chemical Sciences, Bahauddin Zakariya University, Multan, 60800, Pakistan
[c] Research Center for Advanced Materials Science (RCAMS), King Khalid University, P.O. Box 9004, Abha 61413, Saudi Arabia
[d] Pharmacy Department, Al-Mustaqbal University College, Babylon, Iraq
[e] Department of Dentistry, Al Noor University College, Bartella, Iraq
[f] Department of Chemistry, College of Science, Imam Abdulrahman Bin Faisal University, P. O. Box 1982, Dammam, 31441, Saudi Arabia
[g] Department of Chemistry, Faculty of Science, King Abdulaziz University, P.O Box 80200, Jeddah, 21589, Saudi Arabia
[h] School of Materials Science and Engineering, Yeungnam University, Gyeongsan, Gyeongbuk, 712-749, Republic of Korea
[i] Department of Physics, Faculty of Science, King Khalid University, P.O. Box 9004, Abha, Saudi Arabia

ARTICLE INFO

Keywords:
Nanomaterials
Co-precipitation
Crystal violet
Heterojunction
Composite

ABSTRACT

In this research, a mesoporous rod-shaped ZnO/CuO/CeO_2 n-p-n heterojunction has been designed via a two-step co-precipitation technique for photocatalytic applications. Characterization by powder X-ray diffraction (PXRD), fourier transform infrared spectroscopy (FTIR), UV–Vis, and Scanning Electron Microscopy (SEM) techniques confirmed the formation of mesoporous rod-shaped ZnO/CuO/CeO_2 n-p-n heterojunction having preferred interface developing between the ZnO, CuO, and CeO_2 phases, thus extended the light-absorption window up to 800 nm. Under sunlight, the ability of a mesoporous ZnO/CuO/CeO_2 n-p-n heterojunction to act as a photocatalyst was tested with methyl orange (MO) and crystal violet (CV) as target molecules. We found the degradation efficiencies of CV and MO dyes on mesoporous ZnO/CuO/CeO_2 to be 96% and 88%, respectively, after 90 min of sunlight irradiation. The estimated rate constants (k, min^{-1}) for deterioration of CV and MO under sunlight over ZnO/CuO/CeO_2 composite were 0.039 and 0.022 min^{-1}, respectively. We endorsed the greater photo-response, the well-aligned band-structure, and practical usage of the photo-induced carriers of the mesoporous photocatalyst to be the leading causes for the outstanding photocatalytic properties of ZnO/CuO/CeO_2 n-p-n heterojunction. The ultimate oxidizing species that destroyed dyes were O_2^- and ·OH over ZnO/CuO/CeO_2 photocatalyst under sunlight illumination. Besides, the recycling tests confirmed the high photostability of the ZnO/CuO/CeO_2 photocatalyst. Hopefully, the mesoporous rod-shaped architecture of the n-p-n heterojunction with anticipated interface manufacturing will assist the photocatalyst strategy with better photocatalytic action under sunlight irradiation.

1. Introduction

Heterojunction nanomaterials like n-p-n and p-n-p were introduced after the discovery of n-p and p-n junctions [1,2]. Currently, interests have been grown in n-p-n and p-n-p nanomaterials that focus on producing enormous knowledge related to operational photocatalytic direct sunlight systems, which have established prospective research in different fields [3,4]. Under sunlight, a single metal-oxide (n-type or p-type) based system is unsuitable for attaining high catalytic efficiency since sunlight photo-activity highly depends on bandgap, e^-/h^+ recombination, and redox potential. So, some changes were made, such as making n-p or p-n junctions, doping, polymer composites, co-doping, and other types of heterojunction, to speed up charge transfer. This made the catalyst work better in sunlight because there was less e^-/h^+

* Corresponding author.
** Corresponding author.
E-mail addresses: Muhammad.aadil@iub.edu.pk (M. Aadil), zahid.smr@yu.ac.kr (M.Z. Ansari).

https://doi.org/10.1016/j.ceramint.2022.09.375
Received 28 August 2022; Received in revised form 27 September 2022; Accepted 30 September 2022
Available online 8 October 2022
0272-8842/© 2022 Elsevier Ltd and Techna Group S.r.l. All rights reserved.

recombination [5–9].

ZnO (n-type), CuO (p-type), and CeO_2 (n-type), as three renowned semiconducting metal oxides, have been expansively explored in the domains of solar-cells, antibiotics, gas-sensors, and photocatalysis due to their amazing optical and electronic properties [10–14]. Out of these, ZnO-based catalysts gained more interest due to their uniqueness: no toxicity, low cost, high photo-oxidization, and high photostability [15]. However, due to its large bandgap (3.37 eV), ZnO has a poor photo-response to sunlight. Rapid e^-/h^+ pair recombination significantly reduces its quantum efficiency, limiting its widespread applications for hydrogen generation, cleaning the environment, and solar energy conversion [10]. With the intention of quenching the recombination photo-induced charges and enhancing the photocatalytic activity of ZnO, substantial research work has been done to make exceedingly effective zinc oxide-based photocatalysts by surface sensitization, doping, and combining of semiconductors and metal deposition [16–18]. Particularly, the coupling of semiconductors is thought to be a good approach to lengthen the separation of e^- and h^+ pair and raise the quantum yield of ZnO. The resulting photocatalysts have been shown to work very well in photocatalysis [19,20].

Copper oxide, a smaller bandgap (1.3–1.8 eV) p-type semiconductor, has prompted prevalent attention due to its assorted applicability in gas sensing, photo-conductivity, and electrochemistry, where the other features of sufficient availability and non-toxicity boost its potential [21, 22]. Despite the great conceivability in the visible spectral region, the photocatalytic action demonstrated by pristine CuO is unexpectedly not pleasing because it is basically suppressed by prompt recombination of the photo-induced e^-/h^+ pair. Hence, to attain high photocatalytic efficacy, a synergic approach could be envisaged through pairing zinc oxide with copper oxide, where copper oxide performing as a co-catalyst might increase the visible light sensitivity. Additionally, the probable construction of auspicious n-p or p-n junctions at the heterostructure interfaces quenches the photo-induced e^-/h^+ recombination and hence offers better performance [23–26]. Cerium oxide (CeO_2), a wide bandgap (2.6–3.4 eV) n-type metal oxide, is also extensively studied for its distinctive electronic, optical, and catalytic properties and various favorable applications in energy and environmental areas. Similarly, combining CuO with CeO_2 to form the heterostructure (CeO_2/CuO) has gained much consideration. It is claimed that this combination can make CeO_2's catalytic action much stronger. This is because the different band edges of CuO and CeO_2 make the charge carrier separation stronger, which leads to the formation of a cascading structure [27–29].

In light of the foregoing analysis, the development of n-p or p-n heterojunction by joining two metal oxides (e.g., ZnO/CuO and CeO_2/CuO) has drawn great attention, and the photocatalytic materials have also been immensely fabricated by various synthetic means. In the current research, we reported on the mesoporous rod-shaped ZnO/CuO/CeO_2 n-p-n heterojunction by combining ZnO with both CuO and CeO_2 via a simple two-step co-precipitation chemical route. Our results inferred that the integration of ZnO, CuO, and CeO_2 as a complex n-p-n heterojunction system may expand the light absorbance response to the visible range and that the catalytic efficiency is substantially improved because of the rapid electron transfer across the potential interfacial gradient in the n-p-n heterojunction. Furthermore, the structure, composition, morphology, and optical absorption were thoroughly examined. The liquid-phase photodegradation of CV and MO as sample pollutants is selected to estimate the catalytic action of the synthesized mesoporous n-p-n heterojunction. The novel aspect of the present study is that we combined three semiconducting metal oxides with different energy levels to develop a ternary-hybrid photocatalyst that not only facilitated the rapid transfer of photo-generated charges but also reduced the probability of electron-hole recombination, thereby enhancing its photocatalytic activity.

2. Experimental

2.1. Chemicals

The precursors such as cerium-nitrate hexahydrate [$Ce(NO_3)_3.6H_2O$, 99.9%], hydrated copper-nitrate [$Cu(NO_3)_2$. xH_2O, ≥ 97%], hydrated zinc-nitrate [$Zn(NO_3)_2$. xH_2O, ~98%], and sodium hydroxide [NaOH, 97%] were used for the preparation of the ZnO/CuO/CeO_2 n-p-n heterojunction. Sodium oxalate [$Na_2C_2O_4$, 99%], *t*-butyl alcohol [$(CH_3)_3COH$, ≥ 99.5%], 1,4-benzoquinone [$C_6H_4O_2$, 99%] crystal violet [$C_{25}N_3H_{30}Cl$], and methyl orange [$C_{14}H_{14}N_3NaO_3S$] were used for photocatalysis studies. Every sort of substance was procured from Merck.

2.2. Synthesis of ZnO/CuO/CeO_2 n-p-n heterojunction

The precipitation approach was adopted to make ZnO/CuO/CeO_2 n-p-n heterojunction [30]. The chemical precipitation technique is used due to its amazing features, easy accessibility, and low-cost preparation. Firstly, in three 500 mL beakers, Ce-nitrate hexahydrate, Cu-nitrate hexahydrate, and Zn-nitrate hexahydrate of 0.15 M were dispersed independently in 200 mL volume of distilled water. Secondly, the precipitation involved the addition of an alkaline solution (0.1 M NaOH) drop by drop into the precursor solutions with persistent stirring. Simultaneously, the pH of the solutions was controlled and adjusted to 9. Thirdly, the three types of precipitate were transferred to another 1000 mL beaker and continuously mixed at 75 °C for 4 h. Then, the product was carefully washed and dehydrated at 130 °C. To finish, the dry powder was sintered at 800 °C to obtain a ZnO/CuO/CeO_2 n-p-n heterojunction.

2.3. Characterizations

The phase development of ZnO/CuO/CeO_2 n-p-n heterojunction was examined by Philips/PANalytical (X'Pert PW 3040) X-ray apparatus using monochromatic Cu-Kα radiations (λ = 0.15406 nm). PXRD data was recorded in the angle (2θ) span of 25°–80° at a scanning rate of 0.05°/s. The FTIR spectrum of ZnO/CuO/CeO_2 n-p-n heterojunction was examined on Spectrum 100 FT-IR (PerkinElmer) within the frequency span of 4000–400 cm^{-1}. The UV–vis absorbance spectrum of ZnO/CuO/CeO_2 n-p-n heterojunction was recorded on a Shimadzu (UV–2501PC) spectrometer within the range of 200 nm–800 nm.

2.4. Photocatalytic tests

The photodegradation of CV (10 mg/L) and MO (10 mg/L) dye was investigated by using ZnO/CuO/CeO_2 n-p-n heterojunction under direct sunlight irradiation. Typically, 50 mL of aqueous suspensions of dyes (CV and MO) and 10 mg of ZnO/CuO/CeO_2 heterostructured powder were added to a 100 mL glass beaker. Prior to sunlight exposure, the mixture was stirred for half-hour to acquire the balance of adsorption-desorption of dyes onto the photocatalyst in the dark. Then the suspensions were exposed to sunlight for 90 min. The absorbance of CV and MO solutions, which were taken out and centrifuged for 10 min, was examined using a UV–vis spectrophotometer. The characteristic absorption wavelengths of CV and MO were 590 nm and 471 nm, respectively. The degree of CV and MO removal could be estimated according to the following expression [31,32]:

$$\boldsymbol{C} = (\boldsymbol{A_0} - \boldsymbol{A_t} / \boldsymbol{A_0}) \times \mathbf{100} \quad (1)$$

Where *C*, A_t, and A_0 are the decolorization degree, initial absorbance, and interval absorbance, respectively. Actually, absorption vs. concentration of CV and MO dyes shows a linear relation in photocatalysis experiments under similar conditions. Thus, the degree of CV and MO decolorization may show their photocatalytic activity.

3. Results and discussions

3.1. Crystalline structure

The crystalline phase of the as-synthesized ZnO/CuO/CeO_2 n-p-n heterojunction was inspected via PXRD measurement, and the typical PXRD pattern is exhibited in Fig. 1. As anticipated, the PXRD micrograph of ZnO/CuO/CeO_2 n-p-n heterojunction contained almost all major diffraction peaks equivalent to ZnO, CuO, and CeO_2 phases. More precisely, high intensity and visible peaks (indicated by Ce) at 28.53° (111), 32.99° (200), 47.41° (220), 56.35° (311), 59.13° (222), 69.56° (400), 76.64° (331) and 79.08° (420) suggested the development of a cubic phase of CeO_2 (Ref. Pattern: 00-004-0593). The peaks at 35.54° (−111), 38.79° (111), 48.74° (−202), 53.97° (020), 58.33° (202), 61.71° (−113), 66.26° (022) and 68.05° (220) (indicated by Cu) were comparable with cubic CuO (Ref. Pattern: 00-001-1117). However, the low intensity peaks at 31.69° (110), 34.58° (002), 36.37° (101), 47.54° (102), 56.58° (110), 62.83° (103), 66.54° (200), 68.11° (112), 69.76° (201), and 77.58° (202) (indicated by Zn) inferred the formation of hexagonal ZnO (Ref. Pattern: 00-005-0664). Clearly, the presence of CeO_2 and CuO reduced the crystallinity of ZnO in ZnO/CuO/CeO_2 nanocomposite. As revealed in Fig. 1, no additional phase was witnessed in the PXRD micrograph of ZnO/CuO/CeO_2, which indicates the high purity of ZnO/CuO/CeO_2 hybrid.

It is important to note that the crystallinity and purity of a nanocomposite photocatalyst are of great importance, as the nanocomposite showing high crystallinity is expected to show superior photodegradation efficiency. The unit-cell parameters (cell side-lengths, cell volume) of three phases (hexagonal, monoclinic, and cubic) that have been developed in a single nanocomposite were estimated via Unit-Cell-software and are given in Table 1. Clearly, the cell side-lengths and volumes were a = 3.464, c = 4.922, V = 51.157 for the ZnO phase, a = 4.719, b = 3.405, c = 5.108, V = 80.910 for the CuO phase, and 5.411, V = 158.438 for the CeO_2 phase in the ZnO/CuO/CeO_2 nanocomposite. The cell side lengths of nanocomposite phases are fairly close to the cell parameters of standard characterized ZnO (00-005-0664), CuO (00-001-1117), and CeO_2 (00-004-0593) minerals, which confirmed the successful growth of three phases in a single nanocomposite. The Debye Scherrer (De.S) formula was applied for the determination of grain size values of the ZnO, CeO_2 and CuO in the ZnO/CuO/CeO_2 nanocomposite [33–36].

$$\textit{Average crystallite size} = k\lambda/\beta \cos\theta \tag{2}$$

Where, D, k, λ, and θ are the crystallite size, shape factor (~0.94), X-ray wavelength, and Bragg's angle, respectively. The De. S crystallite size of ZnO, CuO, and CdO was determined to be 19.82, 36.19, and 19.88 nm, respectively. Similarly, the Williamson's Hall (Wi. H) expression was also applied to estimate the crystallite sizes and strain for ZnO, CuO, and CeO_2 in the nanocomposite [37].

$$\beta \cos\theta = \frac{k\lambda}{D} + 4\varepsilon \sin\theta \tag{3}$$

$$\varepsilon = \beta s / 4 \tan\theta \tag{4}$$

By plotting $\beta \cos\theta$ verses$4\varepsilon \sin\theta$, the intercept values were found by linear fitting (Fig. 2 (a-c), which was then applied for the estimation of Wi. H crystallite sizes. The estimated values of crystallite sizes and strain by **Eq. (3)** and **Eq. (4)** are given in Table 1. By comparing the Wi. H crystallite size values with the De. S crystallite size values, it was noted that they are much closer to each other.

Furthermore, the crystallite size values were inverted and squared to obtain the dislocation density values for ZnO, CuO, and CeO_2 phases in the nanocomposite.

$$\delta = 1/D^2 \text{lines}/m^2 \tag{5}$$

Where, δ and D represent the dislocation density and crystallite size, respectively.

3.2. FTIR analysis

From the FTIR characterization, the types of bonding and presence of different functional groups in the prepared materials can be revealed. Fig. 3 displays the FTIR spectrum of the as-synthesized ZnO/CuO/CeO_2 n-p-n heterojunction within the 4000-400 cm^{-1} range at high resolution.

All the FTIR peaks that have appeared due to Zn–O, Ce–O and Cu–O metal oxide bonds and other surface adsorbed molecular vibrations are properly labeled. The FTIR broad peak that appeared around 3600–3300 cm^{-1} is allotted to the stretching-mode of oxygen-hydrogen bonds residing on the outer surface of the ZnO/CuO/CeO_2 nanocomposite sample [38]. However, the peak at 1627 cm^{-1} has been referred to the bending-mode of H–O–H (surface-attached H_2O molecules) [39]. Furthermore, the peaks at 1138 cm^{-1} and 1564 cm^{-1} signify the *C*–O stretching-mode and C═O symmetric stretching-mode, respectively. The sharp peaks at 498–521 cm^{-1} and 456-475 cm^{-1} were assigned to the copper-oxygen and zinc-oxygen stretching-modes, but peaks detected at 536 cm^{-1} and 583 cm^{-1} were designated to the stretching-mode and bending-mode of the Ce–O bonds. In Fig. 3, the presence of vibrational bands in the 1000–400 cm^{-1} range confirms the formation of a ZnO/CuO/CeO_2 n-p-n heterojunction.

3.3. SEM analysis

The SEM technique was applied to examine the formation of ZnO/CuO/CeO_2 n-p-n heterojunction, and the resulting micrograph is shown in Fig. 4. The typical SEM micrograph explains that the precipitation reaction generates predominantly randomly distributed mesoporous rods with distinct facets. It is evident that mesoporous rods have mainly hexagonal cross-sections. The mesoporous rods have diameters of one to 2 μm and lengths in the range of several micrometers. The rods' mesoporous structure will give them a lot of places where pollutant molecules

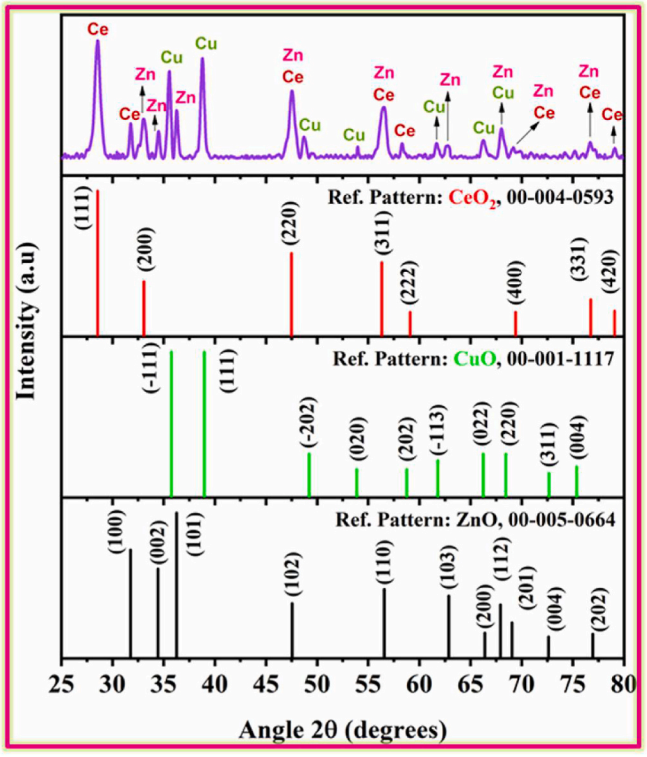

Fig. 1. PXRD micrograph of ZnO/CuO/CeO_2 n-p-n heterojunction.

Table 1
Lattice parameters (Cell side-lengths and Cell volume), average crystallite sizes (Wi.H and De.S), dislocation density, and strain of ZnO/CuO/CeO_2 nanocomposite.

Samples	*Phase*	*Cell side lengths*			*Cell Volume(Å)^3*	*Crystallite Sizes (nm)*		*Dislocation Density δx10^{14}(line/m^2)*	*Strain Ɛx10^{-4}*
		a(Å)	*b(Å)*	*c(Å)*		*De.S*	*Wi.H*		
ZnO/CuO/CeO_2	ZnO	3.464	3.464	4.922	51.157	19.82	18.75	25.45	36.0
	CuO	4.719	3.404	5.108	80.910	36.19	31.24	7.635	0.04
	CeO_2	5.411	5.411	5.411	158.44	19.88	19.90	25.30	8.04

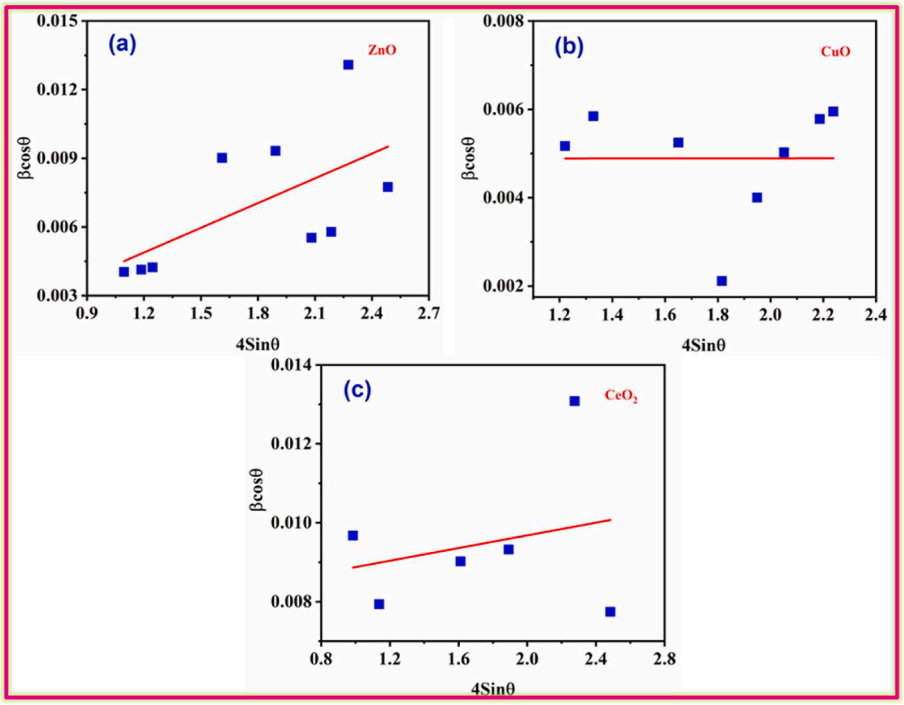

Fig. 2. Williamson-Hall plots of ZnO, CuO, and CeO_2 existing within ZnO/CuO/CeO_2 n-p-n heterojunction.

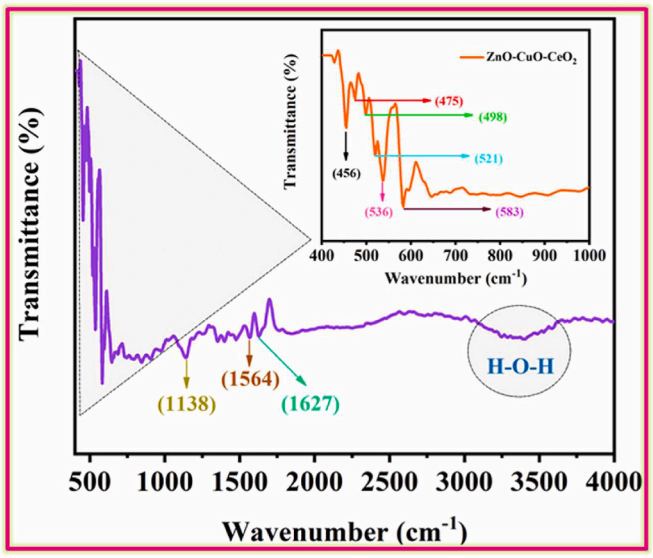

Fig. 3. FTIR spectrum of ZnO/CuO/CeO_2 n-p-n heterojunction.

can stick to and be broken down by light.

In evaluating the photocatalytic ability of a prepared photocatalyst, the wavelength range in which it absorbs light radiation is considered an important constraint [40]. So, the UV–Vis analysis (200 nm–800 nm wavelength range) was used to check the optical property of the ZnO/CuO/CeO_2 n–p–n heterojunction that was made, as shown in Fig. 5a.

The absorption peaks for the ZnO/CuO/CeO_2 nanocomposite showed that it responds to visible light due to the interlacing of three metal oxides. The mutual incorporation of ZnO, CuO, and CeO_2 metal oxides developed a heterostructured nanocomposite and caused a wide visible absorption. The visible light absorptions were seen at 354 nm and 413 nm for the ZnO/CuO/CeO_2 nanocomposite in contrast to bulk ZnO, CuO, and CeO_2. However, visible absorption was also noticed at 290 nm for the nanocomposite. So, the UV–Vis activation of ZnO/CuO/CeO_2 n-p-n heterojunction in sunlight will help in boosting its photocatalytic efficiency. The optical response and bandgap energy of ZnO/CuO/CeO_2 hybrid were examined via Tauc plot expression was used which is revealed in Eq. (6) [[41,42]].

$$ahv = A\left(hv - E_g\right)^n \tag{6}$$

Where α, *A*,.*h*, and *v* indicate the absorbance coefficient, proportionality constant, Plank's constant, and photon's frequency, respectively. Optical bandgap energy was denoted by E_g, and exponent 'n' was a result of the direct, indirect, forbidden direct, and forbidden indirect (n = 2, 1/2, 3, and 3/2) electronic transitions [43]. From optical observation, n = 1/2 (direct electronic transition) was taken for ZnO/CuO/CeO_2 n-p-n heterojunction. A Tauc plot is displayed in Fig. 5b, and the obtained bandgap of the nanocomposite is 2.41 eV. So, the nanocomposite might be stimulated via visible light, and it is anticipated that ZnO, CuO, and CeO_2 are incorporated well in the ZnO–CuO–CeO_2. The presence of ZnO,

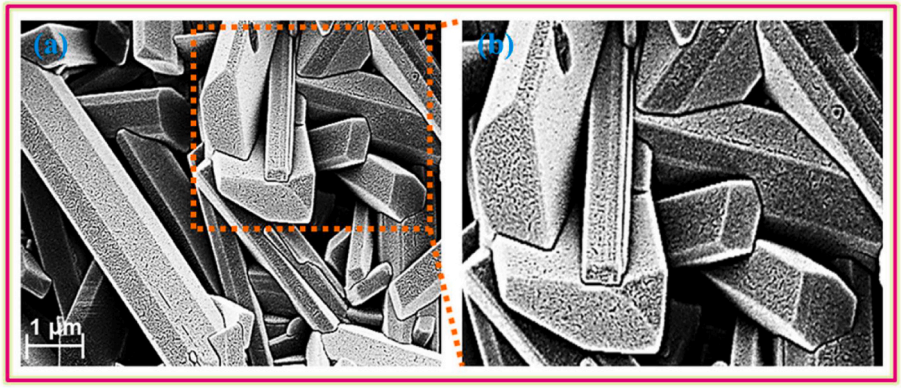

Fig. 4. (a) SEM micrograph of ZnO/CuO/CeO_2 n-p-n heterojunction and (b) enlarged view. **Optical study**.

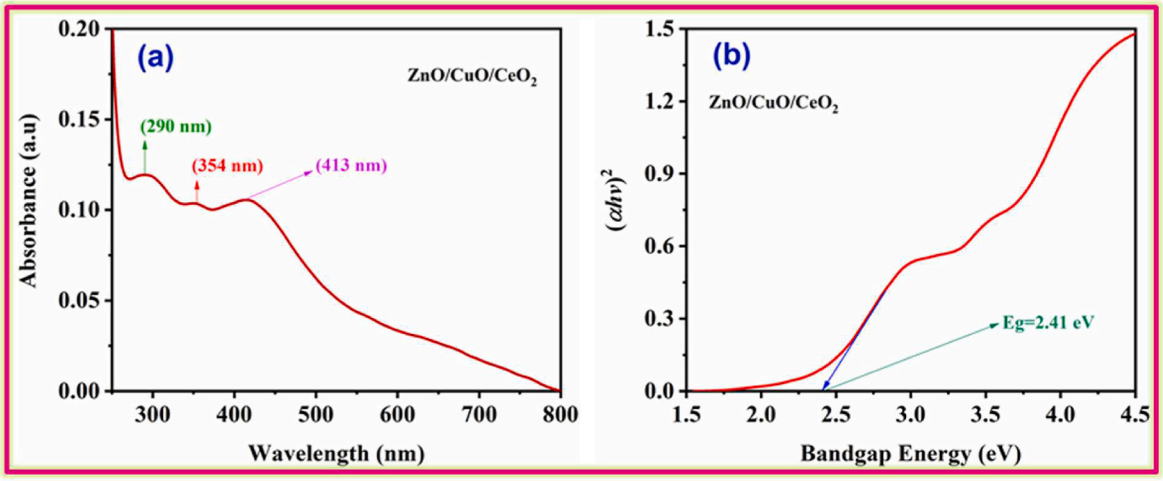

Fig. 5. (a) UV–Vis absorbance plot and (b) Bandgap plot of ZnO/CuO/CeO_2 n-p-n heterojunction.

CuO, and CeO_2 in a single nanocomposite causes a shift in Fermi levels of conduction. This shift enables the visible-light irradiation to excite valence band electrons into the conduction band easily. This way, the AOP efficiency of the nanocomposite could be readily enhanced under the impact of visible radiation. The optical study confirmed that ZnO/CuO/CeO_2 n-p-n heterojunction is a prospective candidate for environmental applications. The results implied that the catalytic efficacy of ZnO/CuO/CeO_2 will be greater than that of another nanocomposite.

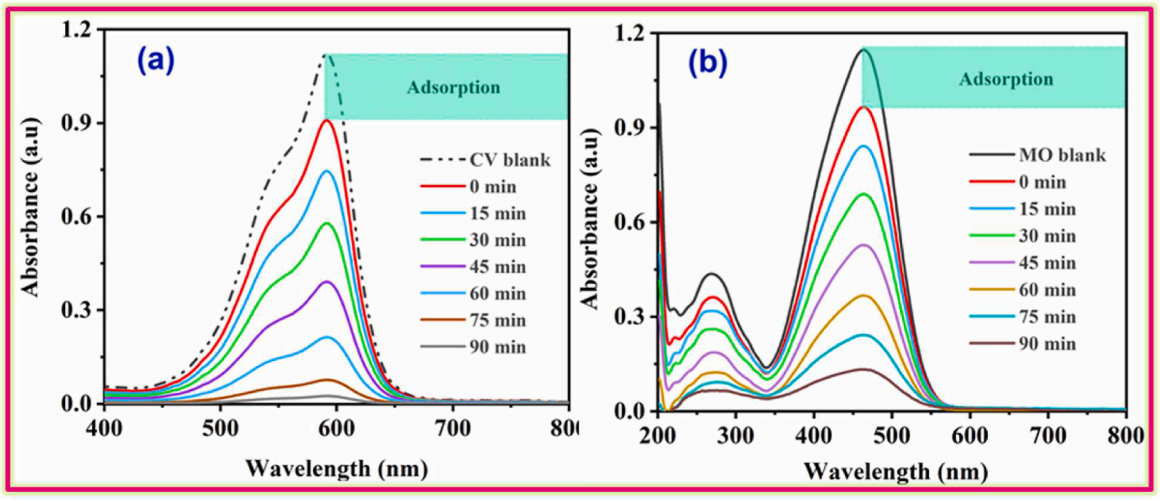

Fig. 6. UV–Vis absorption profiles of (a) CV and (b) MO degradation over ZnO/CuO/CeO_2 n-p-n heterojunction under sunlight irradiations.

3.4. Photocatalytic study

From the prevalent applications of CeO_2 and ZnO nanostructures, their usage for ultra-violet light-driven elimination of organic pollutants has become a hotspot of current research. Likewise, CuO nanomaterials also exhibited their fitness as a photocatalytic material in visible light exposure. So, by comprehending heterostructures consisting of these three metal-oxides, we may anticipate an improvement in photocatalytic activity due to the usage of the entire solar-light spectrum. The photocatalytic performance of ZnO/CuO/CeO_2 n-p-n heterojunction was measured with CV and MO as target molecules under sunlight exposure. The development of the UV–vis absorbance plots of CV and MO at fixed interims as the outcome of the photodegradation efficiency of ZnO/CuO/CeO_2 nanocomposite under sunlight is given in Fig. 6a, b. A steady decrease in the intensity of λ_{max} of CV and MO at 590 nm and 461 nm with the passage of time was seen, and after 90 min, the λ_{max} intensities were decreased by 96% (CV) and 88% (MO).

For the quantitative study of the photodegradation performance, the decrement in dye contents (C_t/C_0) was plotted against irradiation time (t) for ZnO/CuO/CeO_2 n-p-n heterojunction (Fig. 7a), where C_0 and C_t denote the initial concentrations after adsorption (t = 0) and final concentrations (t = t) of CV and MO dyes, respectively.

The CV and MO dye contents in the reaction suspensions were directly related to their λ_{max} intensity. Therefore, the C_t/C_0 is identical to the absorbance ratio at irradiation time t = t and t = 0. From Fig. 7a, the high photodegradation ability of ZnO/CuO/CeO_2 n-p-n heterojunction for CV dye contrary to MO dye can be perceived very remarkably. The photodegradation witnessed for CV and MO dyes by sunlight irradiation followed pseudo-first-order kinetics [44–46].

$$\ln(C_t / C_0) = k_{app} C \quad (7)$$

By plotting ln (C_t/C_0) and irradiation time (t), the k_{app} value for CV and MO degradation over ZnO/CuO/CeO_2 n-p-n heterojunction was estimated (Fig. 7b). The value of k_{app} for CV disintegration was estimated to be 1.73 times higher than MO degradation over ZnO/CuO/CeO_2 n-p-n heterojunction (**Table 2**).

Moreover, for a simplistic relative view, CV and MO photodegradation percentages over ZnO/CuO/CeO_2 nanocomposite after 90 min of sunlight exposure are plotted in Fig. 7c. The enhanced photodegradation efficiency of ZnO/CuO/CeO_2 nanocomposite under sunlight may be explored by various factors. Firstly, the ZnO, CuO, and CeO_2 forming the n-p-n heterojunction possess UV and visible light absorption (Fig. 5a) and can combine UV and visible activation in photocatalytic reactions. Secondly, a heterostructure with coordinated band structures prevents the speedy recombination of e^-/h^+ pairs, which is perhaps the main cause of the increase in the photodegradation efficiency of ZnO/CuO/CeO_2. The suppressed recombination of e^-/h^+ pairs permits more photo-generated electrons and holes to contribute not only to the reduction of molecular oxygen to superoxide radicals but also to the oxidation of water molecules and hydroxyl ions to hydroxyl radicals, which are the robust oxidizing agents and can degrade CV and MO dyes effectively. Thirdly, ZnO/CuO/CeO_2 n-p-n heterojunction has a strong capturing ability of cationic (CV) and anionic (MO) dyes, which provides the catalyst a novel capturing event to accumulate the CV and MO molecules onto the catalytic surface and stimulate the degradation efficiency.

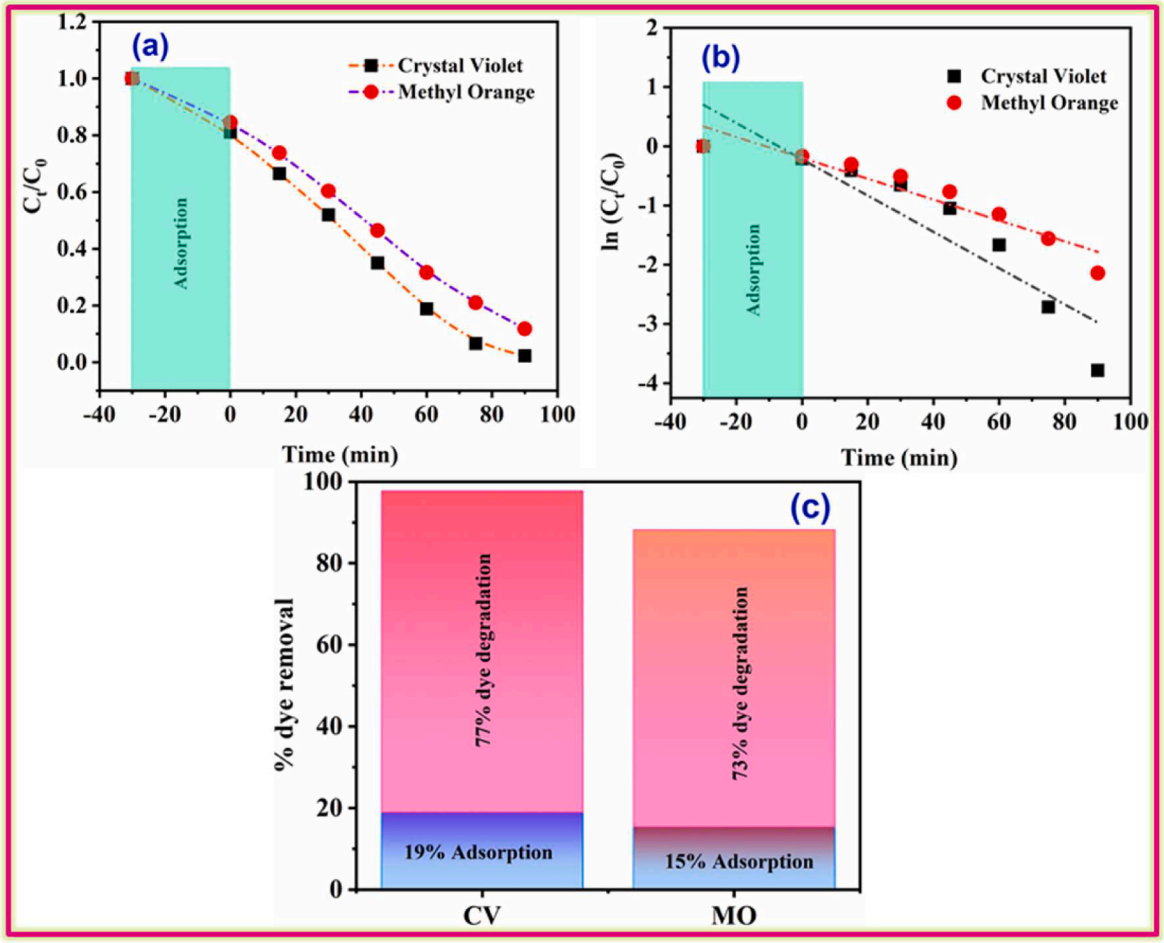

Fig. 7. (a, b) Kinetics profiles and (c) % degradation of CV and MO dyes over ZnO/CuO/CeO_2 n-p-n heterojunction under sunlight irradiations.

Table 2
Kinetics information of ZnO/CuO/CeO_2 n-p-n heterojunction for CV and MO dyes degradation under sunlight irradiations.

Photocatalyst	Dye name	% dye removal	Irradiation time (min)	$_{Kapp}$ (min^{-1})	Half-life $t_{1/2}$ (min)	adj-R^2
ZnO–CuO–CeO_2	MO	88	90	0.022	31.5	0.9426
–	CV	96	90	0.039	17.8	0.8919

The permanence of the photocatalyst, a critical measure for their persistent use in environmental treatment, was then assessed by the photodegradation of CV and MO for three runs with the ZnO/CuO/CeO_2 n-p-n heterojunction. The catalyst sample demonstrated amazingly high-stability in spite of three runs, as illustrated in the deterioration graph in Fig. 8 (a, b).

Under sunlight irradiations for 90 min, i.e., after the initial operational run, the residual CV and MO concentrations were only 2%. A minute reduction (<5%) in photodegradation performance was perceived for ZnO/CuO/CeO_2 n-p-n heterojunction, where the remaining dye concentrations after three operational runs were only <5%. Such a little efficiency decline recommends the extraordinary photo-stability and reusability of the n-p-n heterojunction.

3.5. Mechanism

The sunlight-driven photodegradation of CV and MO over ZnO/CuO/CeO_2 n-p-n heterojunction is likely to be completed in three processes: molecular dye capture, photodegradation, and release [47]. The proposed capture-photodegradation-release mechanism has been illustrated in Fig. 9.

As usual, the CV and MO dye molecules are taken up by the CeO_2 on the external surface of the ZnO/CuO/CeO_2 n-p-n heterojunction and then rapidly degraded under sunlight irradiation, and eventually, the photodegradation products are discharged to the peripheral environment. The special band-structure of ZnO/CuO/CeO_2 n-p-n heterojunction played a primary role in the growth of photocatalytic aptitude for the discoloration of CV and MO solutions. Therefore, the valence and conduction edges positions of metal-oxides in the ZnO/CuO/CeO_2 hybrid were estimated via the following specified equations [48,49]:

$$E_{VB} = \chi - (E_e + 0.5E_g) \quad (8)$$

$$E_{CB} = E_{VB} - E_g \quad (9)$$

Where E_{CB}, X, E_g, E_e, and E_{VB} are the CB potential, Mulliken's electronegativity, bandgap energy, free-electron's energy (4.5 eV), and VB potential, respectively. The tentative band configuration mechanism at the connected interface of ZnO/CuO/CeO_2 n-p-n heterojunction shows the bandgap and charge transfer in the n-p-n heterojunction semiconductor system. The bandgap energies of ZnO, CuO, and CeO_2 semiconductors, taken as 3.2 eV, 2.1 eV, and 3.1 eV, respectively, suggest that the three metal oxides have different band configurations and electron affinities. ZnO has a conduction band position below CeO_2 but above that of CuO. Therefore, a type-II (staggered) heterojunction at the interfacial region of ZnO/CuO/CeO_2 was formed. When ZnO/CuO/CeO_2 n-p-n heterojunction is exposed to sunlight, electrons from VB of CuO move to its CB, while holes remain in VB, and because of the higher Fermi levels of CuO than ZnO and CeO_2, the photo-induced electrons migrate towards the CB of ZnO and CeO_2. In this way, the holes and electrons were separated well at the CuO/ZnO and CuO/CeO_2 interfaces. They react with oxygen molecules and hydroxyl groups to form the superoxide ions ($\cdot O_2^-$) and hydroxyl radicals (·OH), which are mainly responsible for the disintegration of CV and MO dyes in the photoreaction.

Based on the above analyses, we came to the conclusion that combining three semiconducting metal oxides with different energy levels to make a ternary-hybrid photocatalyst can help the fast transfer of photo-generated charges, reduce the chance of recombination, and lengthen the life of charge-carriers, leading to an increase in the photocatalytic action of ZnO/CuO/CeO_2 sample.

4. Conclusions

In summary, a mesoporous rod-shaped ZnO/CuO/CeO_2 n-p-n heterojunction catalyst has been designed via a co-precipitation chemical route for the deterioration of unsafe organic pollutants from polluted waters under sunlight irradiation. The characterization of ZnO/CuO/CeO_2 n-p-n heterojunction via PXRD, FTIR, UV–Vis and SEM techniques provided insight into its microstructure, phase, crystallite size, composition, morphology, and optical properties. PXRD analysis confirmed the development of three distinct phases in the PXRD spectrum of the ZnO/CuO/CeO_2 composite. FTIR and SEM analyses revealed the high purity

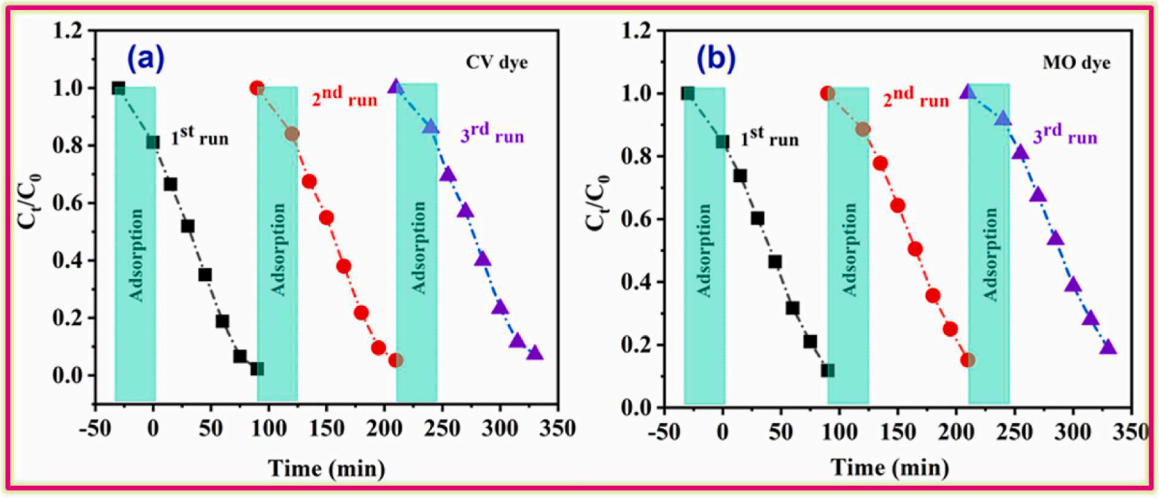

Fig. 8. Cyclic stability of ZnO/CuO/CeO_2 n-p-n heterojunction for crystal violet and methyl orange photodegradation under sunlight irradiations. (For interpretation of the references to color in this figure legend, the reader is referred to the Web version of this article.)

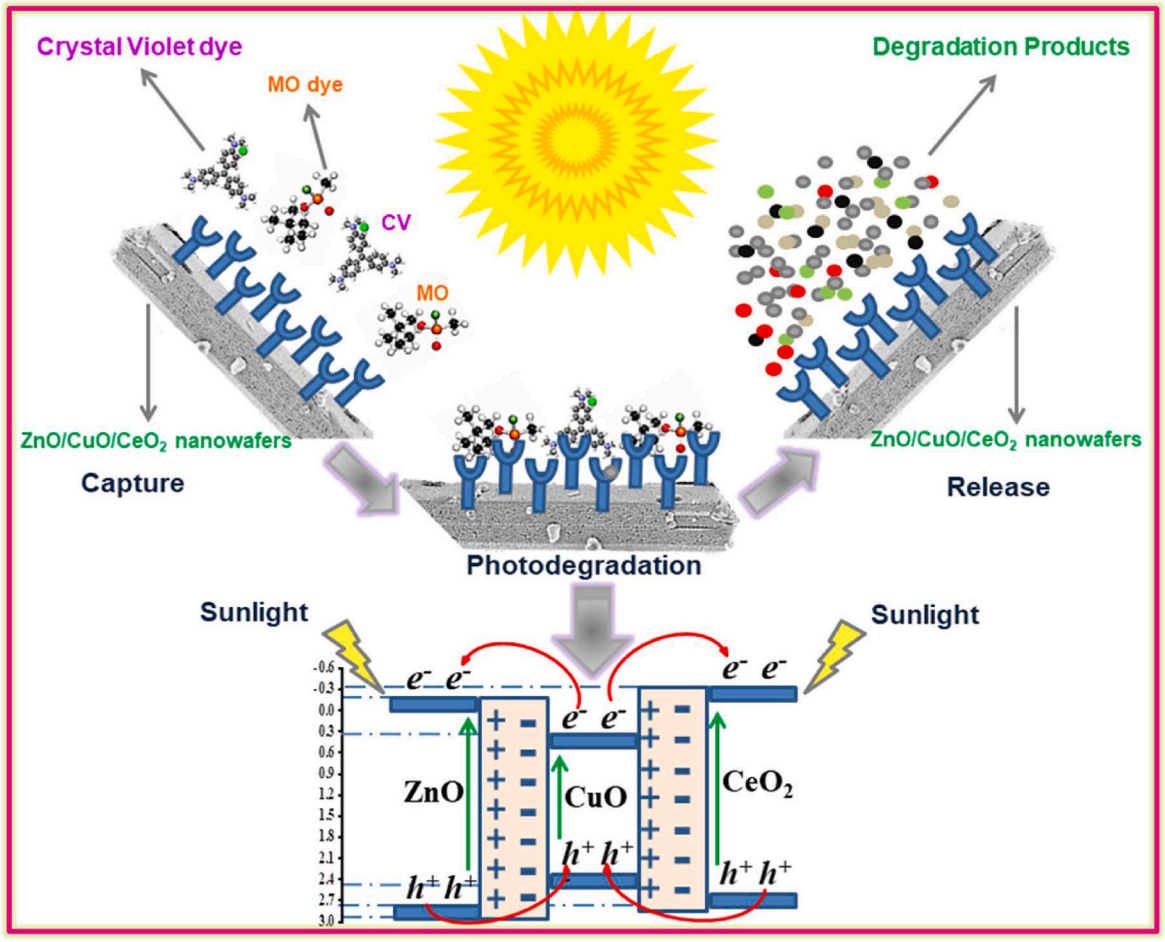

Fig. 9. Representation of the capture-photodegradation-release system of CV and MO photodegradation by ZnO/CuO/CeO_2 nanowafer heterostructure under sunlight irradiations.

with mesoporous rod-shaped morphology. The n-p-n heterojunction was recognized as a highly effective dye degradation photocatalyst under sunlight, with degradation efficiencies of 96% and 88% for CV and MO pollutants, respectively. Interestingly, the mesoporous rod-shaped composite performed better as a catalyst for both cationic (CV) and anionic (MO) dyes, demonstrating the importance of the composite material's size and shape. The n-p-n heterojunction development guided the electrons to gather in the n-type (ZnO and CeO_2) while the holes remained with the p-type (CuO), which further prolonged the charge separation. The better quantum efficiency of ZnO/CuO/CeO_2 was due to the synergy of n-type and p-type semiconductors in expanding the visible light absorbance span up to 800 nm. The overall performance of mesoporous rod-shaped ZnO/CuO/CeO_2 n-p-n heterojunction for cationic and anionic dyes with high-stability holds promise of developing other tertiary-composite stable photocatalysts for environmental remediation.

Declaration of competing interest

The authors declare that they have no known competing financial interests or personal relationships that could have appeared to influence the work reported in this paper.

Acknowledgement

Authors sincerely appreciate the King Khalid University for the research grant (KKU/RCAMS/22) under the Research Center for Advanced Materials Science (RCAMS) at King Khalid University, Saudi Arabia. Authors are also thankful to the Department of Chemistry, The Islamia University of Bahawalpur (RYK-Campus) and Higher Education Commission (HEC)-Islamabad Pakistan.

References

[1] X. Sun, Y. Li, Y. Du, Z. Li, N. Jiang, J. Qu, L. Xue, G. Sun, In situ construction of $Bi_4O_5I_2$-$Bi_2O_2CO_3$-$BiOC_{l0}$. 8I0. 2 npn heterojunction for enhanced photocatalytic performance, Colloids Surf. A Physicochem. Eng. Asp. 626 (2021), 126988.

[2] S. Rajendran, T.K.A. Hoang, M.L. Trudeau, A.A. Jalil, M. Naushad, M.R. Awual, Generation of novel npn (CeO_2-PPy-ZnO) heterojunction for photocatalytic degradation of micro-organic pollutants, Environ. Pollut. 292 (2022), 118375.

[3] P.-Y. Kuang, X.-J. Zheng, J. Lin, X.-B. Huang, N. Li, X. Li, Z.-Q. Liu, Facile construction of dual p-n junctions in CdS/Cu_2O/ZnO photoanode with enhanced charge carrier separation and transfer ability, ACS Omega 2 (2017) 852–863.

[4] U. Kumar, S. Das Chakraborty, R.K. Sahu, P. Bhattacharya, T. Mishra, Improved interfacial charge transfer on noble metal-free biomimetic CdS-based tertiary heterostructure@ 2D MoS2-CdS-Cu_2O with enhanced photocatalytic water splitting, Adv. Mater. Interfac. 9 (2022), 2101680.

[5] Z. Jiang, L. Feng, J. Zhu, B. Liu, X. Li, Y. Chen, S. Khan, Construction of a hierarchical $NiFe_2O_4$/$CuInSe_2$ (p-n) heterojunction: highly efficient visible-light-driven photocatalyst in the degradation of endocrine disruptors in an aqueous medium, Ceram. Int. 47 (2021) 8996–9007.

[6] Q. Yang, Y. Li, Z. Xia, W. Chang, Y. Xing, Preparation of two-dimensional mesoporous Ta_3N_5 by utilizing a biological template for enhanced photocatalytic hydrogen production, Ceram. Int. 48 (2022) 22338–22345.

[7] H. Katsumata, M.A. Islam Molla, J.B. Islam, I. Tateishi, M. Furukawa, S. Kaneco, Dual Z-scheme heterojunction g-C_3N_4/Ag_3PO_4/AgBr photocatalyst with enhanced visible-light photocatalytic activity, Ceram. Int. 48 (2022) 21939–21946.

[8] N.A. Khan, I. Ahmad, N. Rashid, M.N. Zafar, F.K. Shehzad, Z. ullah, A. Ul-Hamid, M.F. Nazar, M. Junaid, M. Faheem, S.S. Shafqat, U. Jabeen, A. Dahshan, Enhanced electrochemical activity of Co_3O_4/Co_9S_8 heterostructure catalyst for water splitting, Int. J. Hydrogen Energy 47 (2022) 30970–30980.

[9] R.S. Gohar, I. Ahmad, A. Shah, S. Majeed, M. Najam-Ul-Haq, M.N. Ashiq, Fabrication of transition-metal oxide and chalcogenide nanostructures with enhanced electrochemical performances, J. Energy Storage 31 (2020), 101621.
[10] A.A. Sumra, M. Aadil, S.R. Ejaz, S. Anjum, T. Saleem, M. Zain, I.A. Alsafari, Biological synthesis of nanostructured ZnO as a solar-light driven photocatalyst and antimicrobial agent, Ceram. Int. 48 (2022) 14652–14661.
[11] C. Gherasim, P. Pascariu, M. Asandulesa, M. Dobromir, F. Doroftei, N. Fifere, A. Dascalu, A. Airinei, Copper oxide nanostructures: preparation, structural, dielectric and catalytic properties, Ceram. Int. 48 (2022) 25556–25568.
[12] M. Shirzad Choubari, J. Mazloom, F.E. Ghodsi, Supercapacitive properties, optical band gap, and photoluminescence of CeO_2-ZnO nanocomposites prepared by eco-friendly green and citrate sol-gel methods: a comparative study, Ceram. Int. 48 (2022) 21385–21395.
[13] X. Wu, L. Yao, M.A. Al-Baadani, L. Ping, S. Wu, A.M. Al-Bishari, K. HiiRuYie, Z. Deng, J. Liu, X. Shen, Preparation of multifunctional drug sustained-release system by atomic layer deposition of ZnO in mesoporous titania coating, Ceram. Int. 46 (2020) 9406–9414.
[14] H. Cheng, J. Hou, Y. Wang, Z. Zhu, Y. Zhang, X. Li, Y. Zhang, Zinc borate modified multifunctional ceramic diaphragms for lithium-ion battery, Ceram. Int. 48 (2022) 24811–24821.
[15] P. Batista-Grau, R.M. Fernández-Domene, R. Sánchez-Tovar, E. Blasco-Tamarit, B. Solsona, J. García-Antón, Indirect charge transfer of holes via surface states in ZnO nanowires for photoelectrocatalytic applications, Ceram. Int. 48 (2022) 21897–21908.
[16] Y. Yulizar Elviera, D.O.B. Apriandanu, R. Marcony Surya, Fabrication of novel $SnWO_4$/ZnO using Muntingia calabura L. leaf extract with enhanced photocatalytic methylene blue degradation under visible light irradiation, Ceram. Int. 48 (2022) 3564–3577.
[17] Y. Liang, W. Li, X. Wang, R. Zhou, H. Ding, TiO_2-ZnO/Au ternary heterojunction nanocomposite: excellent antibacterial property and visible-light photocatalytic hydrogen production efficiency, Ceram. Int. 48 (2022) 2826–2832.
[18] I. Ahmad, M. Aslam, U. Jabeen, M.N. Zafar, M.N.K. Malghani, N. Alwadai, F. H. Alshammari, A.S. Almuslem, Z. Ullah, ZnO and Ni-doped ZnO photocatalysts: synthesis, characterization and improved visible light driven photocatalytic degradation of methylene blue, Inorg. Chim. Acta. 543 (2022), 121167.
[19] C. Li, X. Liu, X. Yang, T. Peng, Y. Li, M. Chen, C. Lin, J. Jiang, Z. Su, W. Kong, Y. Wang, Tetragonal multilayered ZnO/CuO composites derived from Zn- and Cu-containing metal-organic framework: effect of calcination temperature on physicochemical properties and photocatalytic activity, Ceram. Int. 48 (2022) 18460–18467.
[20] Q. Meng, W. Liu, J. Jiang, X. Zhang, Fabrication of novel p-CuO/n-ZnO heterojunction nanofibers by electrospinning for enhanced photocatalytic performance in the denitrification of fuel oil, Ceram. Int. 47 (2021) 19402–19413.
[21] R. Vandamar Poonguzhali, E. Ranjith Kumar, N. Arunadevi, C. Srinivas, M. E. Khalifa, S. Abu-Melha, N.M. El-Metwaly, Natural citric acid assisted synthesis of CuO nanoparticles: evaluation of structural, optical, morphological properties and colloidal stability for gas sensor applications, Ceram. Int. 48 (2022) 26287–26293.
[22] M. Zhang, T. Hu, P. Chang, Z. Jin, H. Mei, N. Dong, L. Cheng, 3D printing of CuO/Cu@Mullite electrodes with macroporous structures and their strong regulation on zinc ion storage, Ceram. Int. 48 (2022) 4124–4133.
[23] F. Cao, T. Wang, X. Ji, Enhanced visible photocatalytic activity of tree-like ZnO/CuO nanostructure on Cu foam, Appl. Surf. Sci. 471 (2019) 417–424.
[24] S. Harish, J. Archana, M. Sabarinathan, M. Navaneethan, K.D. Nisha, S. Ponnusamy, C. Muthamizhchelvan, H. Ikeda, D.K. Aswal, Y. Hayakawa, Controlled structural and compositional characteristic of visible light active ZnO/CuO photocatalyst for the degradation of organic pollutant, Appl. Surf. Sci. 418 (2017) 103–112.
[25] S. Pal, S. Maiti, U.N. Maiti, K.K. Chattopadhyay, Low temperature solution processed ZnO/CuO heterojunction photocatalyst for visible light induced photo-degradation of organic pollutants, CrystEngComm 17 (2015) 1464–1476.
[26] M. Zarei, M. Borhani Zarandi, M. Alizadeh, Preparation of CuO/CeO_2 composites by the Pechini method and investigation of their structural and electrical properties, Ceram. Int. 45 (2019) 1991–1997.
[27] X. Ma, P. Lu, P. Wu, Optical and ferromagnetic properties of hydrothermally synthesized CeO_2/CuO nanocomposites, Ceram. Int. 44 (2018) 5284–5290.
[28] S.-Y. Lin, T.-W. Chiu, C. Dong, Preparation and characterization of $CuCrO_2$-CeO_2 composite nanopowder by a self-combustion glycine nitrate process, Ceram. Int. 43 (2017) S639–S642.
[29] M. Liao, H. Qin, W. Guo, P. Gao, H. Xiao, Porous reticular CuO/ZnO/CeO_2/ZrO_2 catalyst derived from polyacrylic acid hydrogel system on Al_2O_3 foam ceramic support for methanol steam reforming microreactor, Ceram. Int. 47 (2021) 33667–33677.
[30] A. Rahman, S. Zulfiqar, S. Musaddiq, I. Shakir, M.F. Warsi, M. Shahid, Facile synthesis of $Ce_{1-x}Fe_xO_2$/NiO/rGO ternary hybrid heterostructures with enhanced visible light mediated photocatalytic activity for waterborne pollutants, J. Photochem. Photobiol. Chem. 397 (2020), 112583.
[31] M. Sabir, M. Ramzan, M. Imran, S.R. Ejaz, A. Anwar, S. Ahmad, M. Aamir, M. Aadil, Synthesis of $La_{1-x}Gd_xFe_{1-y}Co_yO_3$/r-GO nanocomposite with integrated features for the treatment of hazardous industrial effluents, Ceram. Int. 48 (2022) 9134–9145.
[32] M. Aadil, S. Zulfiqar, M.F. Warsi, P.O. Agboola, I. Shakir, M. Shahid, N.F. Al-Khalli, Mesoporous and macroporous Ag-doped Co_3O_4 nanosheets and their superior photo-catalytic properties under solar light irradiation, Ceram. Int. 47 (2021) 9806–9817.
[33] N.I. Abu-Elsaad, S.A. Mazen, A.Y. Sleem, Production of Cr^{3+} substituted Li-Zn nanocrystalline ferrite by citrate method: studies on structure, cation occupancy, elastic, optical and magnetic performance, Ceram. Int. 48 (2022) 14210–14223.
[34] I. Ahmad, S.M. Shah, M.N. Zafar, S. Ullah, A. Ul-Hamid, M.N. Ashiq, U. Jabeen, M. Shafa, A. Rahdar, Fabrication of highly resistive La-Zn co-substituted spinel strontium nanoferrites for high frequency devices applications, Mater. Chem. Phys. 259 (2021), 124031.
[35] M. Aadil, W. Hassan, H.H. Somaily, S.R. Ejaz, R.R. Abass, H. Jasem, S.K. Hachim, A.H. Adhab, E.S. Abood, I.A. Alsafari, Synergistic effect of doping and nanotechnology to fabricate highly efficient photocatalyst for environmental remediation, J. Alloys Compd. 920 (2022), 165876.
[36] I. Ahmad, S.M. Shah, M.N. Zafar, M.N. Ashiq, W. Tang, U. Jabeen, Synthesis, characterization and charge transport properties of Pr-Ni Co-doped $SrFe_2O_4$ spinel for high frequency devices applications, Ceram. Int. 47 (2021) 3760–3771.
[37] S. Munir, A. Rasheed, S. Zulfiqar, M. Aadil, P.O. Agboola, I. Shakir, M.F. Warsi, Synthesis, characterization and photocatalytic parameters investigation of a new $CuFe_2O_4$/Bi_2O_3 nanocomposite, Ceram. Int. 46 (2020) 29182–29190.
[38] I. Ahmad, J. Ahmed, S. Batool, M.N. Zafar, A. Hanif, Zahidullah, M.F. Nazar, A. Ul-Hamid, U. Jabeen, A. Dahshan, M. Idrees, S.A. Shehzadi, Design and fabrication of Fe_2O_3/FeP heterostructure for oxygen evolution reaction electrocatalysis, J. Alloys Compd. 894 (2022), 162409.
[39] N.A. Khan, N. Rashid, I. Ahmad, Zahidullah, R. Zairov, H.u. Rehman, M.F. Nazar, U. Jabeen, An efficient Fe_2O_3/FeS heterostructures water oxidation catalyst, Int. J. Hydrogen Energy 47 (2022) 22340–22347.
[40] M.A. Sayed, M.M. Abo-Aly, A.A.A. Aziz, A. Hassan, A.N.M. Salem, A facile hydrothermal synthesis of novel CeO_2/CdSe and CeO_2/CdTe Nanocomposites: spectroscopic investigations for economically feasible photocatalytic degradation of Congo red dye, Inorg. Chem. Commun. 130 (2021), 108750.
[41] A. Rahman, R. Afzal, S. Zulfiqar, I.A. Alsafari, M.A. Khan, P.O. Agboola, S. Haider, M.F. Warsi, I. Shakir, Superior photodegradation and antibacterial activity of r-GO supported ternary nanocomposite of doped transition metal compounds, Ceram. Int. 47 (2021) 14569–14578.
[42] H.A. Alburaih, M. Aadil, S.R. Ejaz, W. Hassan, A. Anwar, S. Anjum, S. Aman, M. S. Al-Buriahi, Z.A. Alrowaili, A.V. Trukhanov, Wet-chemical synthesis of urchin-like Co-doped CuO: a visible light trigger photocatalyst for water remediation and antimicrobial applications, Ceram. Int. 48 (2022) 21804–21813.
[43] G.K. Upadhyay, T.K. Pathak, L.P. Purohit, Heterogeneous ternary metal oxide nanocomposites for improved advanced oxidation process under visible light, Cryst. Res. Technol. 55 (2020), 2000099.
[44] A. Rahman, S. Zulfiqar, A.U. Haq, I.A. Alsafari, U.Y. Qazi, M.F. Warsi, M. Shahid, Cd-Gd-doped nickel spinel ferrite nanoparticles and their nanocomposites with reduced graphene oxide for catalysis and antibacterial activity studies, Ceram. Int. 47 (2021) 9513–9521.
[45] T. Kousar, M. Aadil, S. Zulfiqar, H.H. Somaily, W. Hassan, H. Sabeeh, F. Mahmood, Temperature controlled synthesis of Co-Ni mixed ferrite nanostructure for the mineralization of azo dye: a novel and facile approach, J. Alloys Compd. 923 (2022), 166224.
[46] H.A. Alburaih, M. Aadil, W. Hassan, L.S. Amaral, S.R. Ejaz, S. Aman, I.A. Alsafari, Multifunctional Fe and Gd co-doped CeO_2-RGO nanohybrid with excellent solar light mediated crystal violet degradation and bactericidal activity, Synth. Met. 287 (2022), 117093.
[47] J. Tian, Y. Sang, Z. Zhao, W. Zhou, D. Wang, X. Kang, H. Liu, J. Wang, S. Chen, H. Cai, Enhanced photocatalytic performances of CeO_2/TiO_2 nanobelt heterostructures, Small 9 (2013) 3864–3872.
[48] A. Rahman, M. Aadil, M. Akhtar, M.F. Warsi, A. Jamil, I. Shakir, M. Shahid, Magnetically recyclable $Ni_{1-x}Cd_xCe_yFe_{2-y}O_4$-rGO nanocomposite photocatalyst for visible light driven photocatalysis, Ceram. Int. 46 (2020) 13517–13526.
[49] N. Tamam, M. Aadil, W. Hassan, S.R. Ejaz, Z.M. Najm, I.A. Alsafari, S. Aman, A. V. Trukhanov, M.S. Al-Buriahi, I. Boukhris, Surfactant assisted synthesis of nanostructured Mn-doped CuO: an efficient photocatalyst for environmental remediation, Ceram. Int. 48 (2022) 29589–29600.